

A frequency-tunable nanomembrane mechanical oscillator with embedded quantum dots

Xueyong Yuan, Michael Schwendtner, Rinaldo Trotta, Yongheng Huo, Javier Martín-Sánchez, Giovanni Piredda, Huiying Huang, Johannes Edlinger, Christian Diskus, Oliver G. Schmidt, Bernhard Jakoby, Hubert J. Krenner, Armando Rastelli

Angaben zur Veröffentlichung / Publication details:






Yuan, Xueyong, Michael Schwendtner, Rinaldo Trotta, Yongheng Huo, Javier Martín-Sánchez, Giovanni Piredda, Huiying Huang, et al. 2019. "A frequency-tunable nanomembrane mechanical oscillator with embedded quantum dots." *Applied Physics Letters* 115 (18): 181902. <https://doi.org/10.1063/1.5126670>.



A frequency-tunable nanomembrane mechanical oscillator with embedded quantum dots

Cite as: Appl. Phys. Lett. **115**, 181902 (2019); <https://doi.org/10.1063/1.5126670>

Submitted: 05 September 2019 . Accepted: 16 October 2019 . Published Online: 28 October 2019

Xueyong Yuan , Michael Schwendtner, Rinaldo Trotta, Yongheng Huo, Javier Martín-Sánchez , Giovanni Piredda, Huiying Huang, Johannes Edlinger, Christian Diskus, Oliver G. Schmidt, Bernhard Jakoby , Hubert J. Krenner , and Armando Rastelli 



View Online



Export Citation



CrossMark

ARTICLES YOU MAY BE INTERESTED IN

[Twist-angle modulation of exciton absorption in MoS₂/graphene heterojunctions](#)

Applied Physics Letters **115**, 181901 (2019); <https://doi.org/10.1063/1.5116325>

[Linewidth broadening factor of an interband cascade laser](#)

Applied Physics Letters **115**, 181101 (2019); <https://doi.org/10.1063/1.5123005>

[On the origin of dislocation generation and annihilation in \$\alpha\$ -Ga₂O₃ epilayers on sapphire](#)

Applied Physics Letters **115**, 182101 (2019); <https://doi.org/10.1063/1.5120554>

Lock-in Amplifiers up to 600 MHz



Zurich
Instruments



A frequency-tunable nanomembrane mechanical oscillator with embedded quantum dots

Cite as: Appl. Phys. Lett. **115**, 181902 (2019); doi: [10.1063/1.5126670](https://doi.org/10.1063/1.5126670)

Submitted: 5 September 2019 · Accepted: 16 October 2019 ·

Published Online: 28 October 2019








View Online



Export Citation



CrossMark

Xueyong Yuan,^{1,2,3}  Michael Schwendtner,¹ Rinaldo Trotta,^{1,4} Yongheng Huo,^{1,5,6,a)} Javier Martín-Sánchez,^{1,7,8,a)}  Giovanni Piredda,⁹ Huiying Huang,¹ Johannes Edlinger,⁹ Christian Diskus,¹⁰ Oliver C. Schmidt,⁵ Bernhard Jakoby,¹⁰  Hubert J. Krenner,^{2,11}  and Armando Rastelli^{1,a)} 

AFFILIATIONS

¹Institute of Semiconductor and Solid State Physics, Johannes Kepler University Linz, Altenbergerstraße 69, 4040 Linz, Austria

²Lehrstuhl für Experimentalphysik 1 and Augsburg Centre for Innovative Technologies (ACIT), Universität Augsburg, Universitätsstraße 1, 86159 Augsburg, Germany

³School of Science, Nanjing University of Posts and Telecommunications, Nanjing 210023, China

⁴Department of Physics, Sapienza University of Rome, Piazzale Aldo Moro 5, 00185 Rome, Italy

⁵Institute for Integrative Nanosciences, IFW Dresden, Helmholtzstraße 20, 01069 Dresden, Germany

⁶Hefei National Laboratory for Physical Sciences at Microscale, University of Science and Technology of China, Shanghai Branch, Xiupu Road 99, Shanghai 201315, China

⁷Departamento de Física, Universidad de Oviedo, 33007 Oviedo, Spain

⁸Centro de Investigación en Nanomateriales y Nanotecnología, CINN (CSIC—Universidad de Oviedo), El Entrego 33940, Spain

⁹Forschungszentrum Mikrotechnik, FH Vorarlberg, Hochschulstraße 1, 6850 Dornbirn, Austria

¹⁰Institute for Microelectronics and Microsensors, Johannes Kepler University Linz, Altenbergerstraße 69, 4040 Linz, Austria

¹¹Nanosystems Initiative Munich (NIM), Schellingstraße 4, 80799 München, Germany

^{a)}Authors to whom correspondence should be addressed: yongheng@ustc.edu.cn; javiermartin@uniovi.es; and armando.rastelli@jku.at

ABSTRACT

Hybrid systems consisting of a quantum emitter coupled to a mechanical oscillator are receiving increasing attention for fundamental science and potential applications in quantum technologies. In contrast to most of the presented works in this field, in which the oscillator eigenfrequencies are irreversibly determined by the fabrication process, we present here a simple approach to obtain frequency-tunable mechanical resonators based on suspended nanomembranes. The method relies on a micromachined piezoelectric actuator, which we use both to drive resonant oscillations of a suspended Ga(Al)As membrane with embedded quantum dots and to fine-tune their mechanical eigenfrequencies. Specifically, we excite oscillations with frequencies of at least 60 MHz by applying an AC voltage to the actuator and tune the eigenfrequencies by at least 25 times their linewidth by continuously varying the elastic stress state in the membranes through a DC voltage. The light emitted by optically excited quantum dots is used as a sensitive local strain gauge to monitor the oscillation frequency and amplitude. We expect that our method has the potential to be applicable to other optomechanical systems based on dielectric and semiconductor membranes possibly operating in the quantum regime.

Published under license by AIP Publishing. <https://doi.org/10.1063/1.5126670>

Micro- and nanomechanical resonators are widely employed as sensors because of their response to, e.g., electric, magnetic, and optical forces. New avenues for nanomechanical resonators have recently opened up thanks to the demonstrated capability of reaching the vibrational ground state of such systems,¹ and achieving quantum entanglement among remote optomechanical oscillators,² as well as from the combination of such mesoscopic objects with two-level quantum

systems.^{3,4} Ideas range from mechanical control of quantum mechanical systems such as single spins,⁵ quantum nondemolition (QND) measurements of the state of the quantum systems by reading the mechanical state of the resonator,⁶ to the use of mechanical oscillations to mediate the interaction between distinct quantum mechanical systems.^{7,8}

For some applications relying on multiple resonators, such as in Ref. 2, it would be useful to have oscillators featuring the same

eigenfrequencies, which is particularly challenging for resonances with high quality (Q) factors, due to unavoidable fluctuations in the fabrication process. In general, precise frequency control is also useful to reduce mechanical dissipation^{9,10} and may play a role in the synchronization of multiple resonators in optomechanical networks.^{11–13} The eigenfrequencies of an oscillator not only are determined by the geometrical parameters and mass density but can also be controlled after fabrication.¹⁴ Fine tuning of the mechanical resonances has been achieved by changing the oscillator temperature¹⁵—an approach poorly suited for oscillators operating in the quantum regime—and also by optical forces¹⁶ and electrostatic^{17–22} forces or by thin-film piezoelectric²³ actuation.

Here, we demonstrate frequency tuning by employing a micro-machined piezoelectric actuator²⁴ capable of inducing large and reversible uniaxial stress on an overlying membrane, with strain values exceeding 1% also at cryogenic temperatures. For a proof of principle, we employ doubly clamped beam oscillators with a mass of a few hundred picograms made of Ga(Al)As, which are directly bonded onto the actuator. The choice of this material class is motivated by their compatibility with complex optomechanical-circuit fabrication²⁵ and with monolithic integration of high-quality quantum dots (QDs).^{3,26,27} Specifically, we use single InGaAs and GaAs quantum dots (QDs) to monitor the vibrations. We also show that the actuator can be easily used to drive oscillations with frequencies of at least 60 MHz, which is already more than one order of magnitude larger than the frequencies explored so far in QD-nanomechanical systems.^{26–28} (Higher vibrational frequencies have only been achieved for propagating nanomechanical waves.^{29–31})

The used piezoelectric actuators were derived from 500- μm thick $(1-x)[\text{Pb}(\text{Mg}_{1/3}\text{Nb}_{2/3})\text{O}_3]-x[\text{PbTiO}_3]$ (PMN-PT) plates, which were mechanically lapped and polished down to a final thickness of $\sim 300\text{ }\mu\text{m}$, microprocessed via a femtosecond laser (see Ref. 32) to feature two finger structures, and metallized, as described in Ref. 24.

The semiconductor samples were grown by molecular beam epitaxy (MBE) on GaAs(001) substrates. The optically active layers (with a thickness of $\sim 250\text{ nm}$) containing the QDs were grown on a 100-nm thick $\text{Al}_{0.7}\text{Ga}_{0.3}\text{As}$ sacrificial layer, which can be removed by selective etching, allowing the nanomembranes to be easily released from the substrate. The InGaAs QDs were obtained via the Stranski-Krastanov (SK) growth mode and the GaAs QDs using the local droplet etching method^{33,34} and were placed at the center of the membrane along the growth direction. After growth, standard optical photolithography, metallization with Cr/Au (3/100 nm), and chemical etching were performed to obtain stripe-shaped nanomembranes with a typical size of $4 \times 300\text{ }\mu\text{m}^2$. The metal layer is used as a lithography mask and to displace the QD layer with respect to the whole membrane center (neutral plane), so that the QDs are subject to strain for both longitudinal and transversal oscillations, as discussed later. (The membrane structures can be found in Fig. S1 of the [supplementary material](#).) The long edges of the membranes are parallel to the [100] crystal direction of GaAs to avoid the occurrence of piezoelectric polarization when uniaxial stress is applied for frequency tuning. After that, the nanomembranes were bonded onto the PMN-PT actuator via a flip-chip process, with the stripes placed on the gap between the finger structures. SU8 photoresist was used as a glue for its strong adhesiveness at relatively low temperature.³⁵ Substrate removal via wet chemical etching leaves suspended membranes, which we use as frequency-tunable

micromechanical oscillators, see Fig. 1. For more detailed information about the device process, see Refs. 24, 36, and 37.

With the PMN-PT actuator, we not only excite mechanical oscillations (as in Refs. 26 and 28), but also tune the intrinsic stress of the nanomembranes (as in Ref. 24). To this end, a voltage $V(t) = V_{\text{DC}} + V_{\text{AC}}(t)$ is applied to the bottom sides of the actuator fingers with respect to the top face (grounded) via a bias-tee, inducing a contraction (for $V > 0$) or expansion (for $V < 0$) of the fingers and thus tensile or compressive strain in the suspended membrane, respectively (see Fig. 1). Since the total length of the fingers (3 mm) is much larger than the gap width (20–70 μm), the strain in the membrane is geometrically enlarged compared to the strain in the PMN-PT.²⁴

To monitor the oscillations, we use the high strain sensitivity of the optical emission of the QDs embedded in the oscillator.^{26,28,38} To this end, we excite photoluminescence (PL) from single QDs at a sample temperature of $\sim 8\text{ K}$ using a continuous-wave (cw) laser with a wavelength of 532 nm, focused by a $50\times$ objective with a numerical aperture of 0.42. The PL signal emitted from QDs is collected by the same objective and detected using a liquid-nitrogen-cooled silicon charge-coupled-device (CCD) after being dispersed by a spectrometer equipped with a 1800 grooves/mm grating.

When the nanomembrane runs into a transverse vibrational resonance, mechanical oscillations occur, in which the QDs will be alternatively subject to compressive and tensile strain [illustrated by the finite-element-method simulations in Fig. 2(a)]. By recording PL spectra while scanning the frequency f of the driving signal $V_{\text{AC}}(t) = V_0 \sin(2\pi f t)$, we detect the occurrence of mechanical resonances as a significant strain-induced line broadening, as shown in Figs. 2(b) and 2(c) for the neutral exciton (X) emission of an In(Ga)As QD. The observed line shape stems from the periodic oscillations of the line position, which are averaged over the PL acquisition time ($\sim 1\text{ s}$, which is much larger than the oscillation period $1/f$). Assuming a Lorentzian line shape for the unperturbed QD emission, the time-integrated spectrum $I(E)$ (PL intensity vs emission energy E) for a driving frequency f can be fit with^{26,28,39,40}

$$I = I_0 + f \frac{2A}{\pi} \int_0^{1/f} \frac{w}{4 \times (E - (E_0 + \Delta E \times \sin(2\pi \cdot f \cdot t)))^2 + w^2} dt, \quad (1)$$

where I_0 , A , w , E_0 , and ΔE are a constant offset, the line intensity, the linewidth, the central energy, and the strain-induced energy shift, respectively. Figure 2(b) shows the fit of the emission broadening at

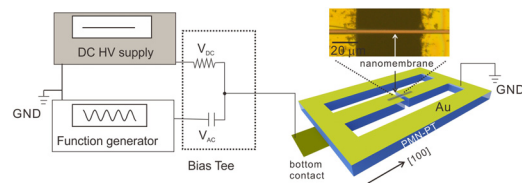


FIG. 1. Schematic drawing of the device and control unit used in this work. A micro-machined PMN-PT actuator is used to both drive oscillations in a mechanical resonator and tune their eigenfrequencies. For a proof of principle, the oscillator consists of a suspended nanomembrane with embedded QDs directly bonded on the two fingers of the PMN-PT actuator. An optical microscopy picture of a finished device is shown in the inset. A DC high-voltage (HV) supply and a function generator are employed to apply DC and AC signals to the bottom contacts of the PMN-PT actuator (extending under the two fingers), while the top face is grounded.

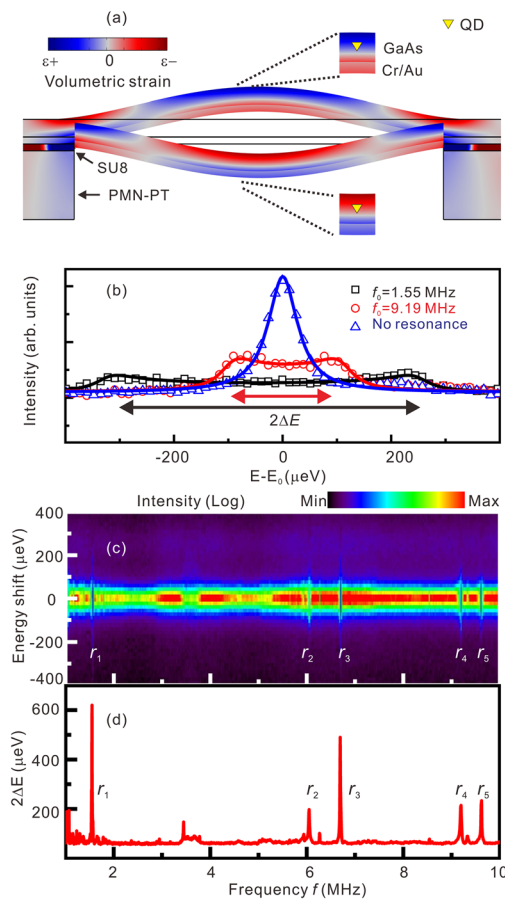


FIG. 2. (a) Finite-element-method calculation of a nanomembrane displacement and strain distribution for the first-order transversal vibration mode. The volumetric strain is color coded (red: compression; blue: tension), and the membrane position is displayed for the situations of maximum displacement. The layer structure includes the semiconductor layer as well as a metal layer (Cr/Au 3/100 nm) and a 100 nm SU8 bonding layer, similar to the experimentally studied membranes (Fig. S1 of the [supplementary material](#)). Due to the off-center position, a QD (indicated by inverted yellow triangles) experiences strain fields, which we detect as emission energy shifts. (b) PL emission of an exciton confined in an InGaAs QD under sinusoidal driving at resonant frequencies $f_0 = 1.55$ MHz, 9.19 MHz, and out of resonance. Solid lines are fits based on Eq. (1), while the off resonance emission is fitted with a Lorentzian. (c) Color-coded plot of the time-integrated emission of the same QD as a function of the driving frequency f between 1 and 10 MHz, with AC driving voltages of $V_0 = 2.0$ V and $V_{DC} = 0$ V. (d) Extracted spectral broadening $2\Delta E$ dependence on the driving frequency f . r_i ($i = 1, 2, \dots, 5$) indicates some of the clearly resolved resonance peaks.

resonant frequencies $f_0 = 1.55$ MHz and 9.19 MHz. Using Eq. (1), we extract spectral broadenings of $2\Delta E = 622$ μeV and 215 μeV for the two resonances, respectively. Figure 2(c) shows the time-averaged PL emission as the frequency f is swept from 1 MHz to 10 MHz, with an AC voltage amplitude of $V_0 = 2.0$ V and no external axial stress applied ($V_{DC} = 0$). The corresponding extracted spectral broadening $2\Delta E$ as a function of frequency f is plotted in Fig. 2(d). At least five sharp resonant peaks [marked as r_i ($i = 1-5$) in Figs. 2(c) and 2(d)] are clearly observable in this range, which indicate distinct mechanical resonances of the suspended nanomembrane. We note here that the pattern of resonances

shows pronounced device-to-device variations (see, e.g., Fig. S4 in the [supplementary material](#)), which we attribute to the simple fabrication process relying on optical lithography and wet etching (which produces fluctuations in the resonator width and side roughness) and the direct bonding to the micromachined actuator (which produces fluctuations in the clamping region and length of the suspended area). Such imperfections and the presence of fabrication-induced stress in the nanomembrane prevent us from ascribing the observed resonances to specific oscillation states. In addition, in the low-frequency range (1–2 MHz), numerous resonances are observed, which we ascribe to electromechanical resonances in the actuator. In addition, we expect longitudinal vibration modes to occur at frequencies above 200 MHz so that we can safely attribute most of the vibration modes in the range between 1 MHz and 10 MHz to transverse modes.

We now turn to the frequency tuning of the mechanical resonances of our simple beam oscillator. Figure 3(a) shows one of the resonances and its evolution with varying driving amplitudes V_0 . Here, a trion emission line of an InGaAs QD is chosen because of its relatively narrow linewidth ($w = 29$ μeV, corresponding to the resolution limit of the used setup) and relatively high intensity. An example of data used to generate Fig. 3(a) is shown in the inset, which presents color-coded PL spectra collected for different driving frequencies with a fixed driving amplitude of $V_0 = 100$ mV. At low driving amplitude, the line shape of the resonance is symmetric, and for $V_{DC} = 0$ V, it has a quality factor of 5446 ± 2 . With increasing driving amplitudes, the peak becomes asymmetric and shifts to lower frequency. This “shark-fin shape” can be attributed to the onset of nonlinear behavior, which can be modeled using a Duffing oscillator model,⁴¹ in which the restoring force has the form $-(k + \alpha x^2)x$, with k and α being the linear and nonlinear elastic constants and x the displacement. Within this model, a redshift can be reproduced by assuming a negative value of α , which indicates a “softening” of the oscillator at large amplitudes. The origin of this behavior, observed for different resonances and devices, is currently not clear.

In order to exclude nonlinear effects and investigate the tuning of the resonance frequency, a smaller driving amplitude of 25 mV is used, which is sufficient to evaluate the tuning behavior when a variable uniaxial stress is introduced by varying V_{DC} . The resonance evolution with different DC voltages (tensile stresses) is plotted in Fig. 3(b). With increasing static tensile stress, the PL emission shows a monotonic redshift, similar to the GaAs QDs studied in Ref. 24. At the same time, the resonance frequency (marked by red dashed circles) increases with increasing tensile stress, as expected from previous works relying on static stress.⁴² This phenomenon can be attributed to a stiffening of the material under tension, which is well known for chord music instruments. Although the frequency tuning shown in Figs. 3(b) and 3(c) is not large ($\sim 0.46\%$, from 2.772 MHz to 2.785 MHz) because of the limited applied V_{DC} (uniaxial strain around 0.03%), the shift is already ~ 25 times larger than the resonance linewidth. In addition, the frequency drifts due to piezocreep are negligible if the system is left to relax for a few minutes after changing the DC voltage: from the data shown in Fig. 3, we extract a drift of up to ~ 0.16 Hz/s for $V_{DC} = 50$ V.

The frequency shift is accompanied by a marked increase in the Q factor from 5446 ± 2 to 7284 ± 2 [shown in Fig. 3(c)], qualitatively consistent with previous results obtained with static tension.^{43–45} Assuming that the Q factor is limited by anchoring losses due to the

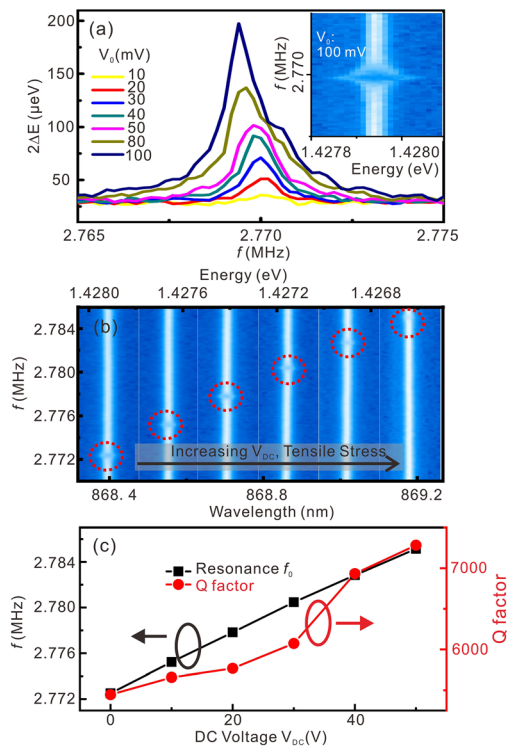


FIG. 3. (a) Variations of the spectral broadening $2\Delta E$ of the trion emission peak from an In(Ga)As QD with different sinusoidal driving amplitudes at a resonant frequency of $f_0 = 2.770$ MHz. The DC voltage was kept at 0 V (no external static axial stress is applied through the PMN-PT actuator). The inset shows the color-coded PL spectra of the trion emission as a function of frequency f for a driving amplitude of $V_0 = 100$ mV. (b) Frequency-resolved PL spectra of trion emission with different tensile stresses. From left to right, the DC voltages were 0, 10, 20, 30, 40, and 50 V. The AC driving amplitude was kept at 25 mV. (c) Resonance f_0 and corresponding Q factor vs DC voltage applied to the actuator fingers (axial stress).

use of a polymer as a bonding layer and possibly by surface losses due to particles and roughness produced by the wet etching process and that such losses are unchanged by the applied static stress, we can qualitatively attribute the increase in the Q factor to “dissipation dilution.”⁴⁶ In a simplistic picture of a damped harmonic oscillator with the equation of motion, $m\ddot{x} + b\dot{x} + kx = f_{drive}$, with m being the oscillator mass, b the dissipation constant, and f_{drive} the driving force, the Q factor is given by $\sqrt{k \times m/b}$, so that an increase in k (and thus of resonance frequency) is also accompanied by an increase in Q.

The reason for the limited tuning range shown here is that often resonances disappeared during the experiment, probably due to irreversible structural changes (for instance, a change in the bonding layer or detachment of particles present on the membrane). In another case, the resonance frequency was changed by as much as 8% (125 kHz) of its original value (1.555 MHz, see [supplementary material Fig. S2](#)). In this case, the estimated strain value is about 0.35%.

Although oscillations are often driven and detected using laser radiation,²⁷ we wish to verify whether it is possible to use our (bulky) PMN-PT actuator to drive oscillations at frequencies closer to the recombination rate of our emitters (~ 1 GHz). Here, we explore the presence of possible resonances on another membrane with GaAs QDs

up to ~ 100 MHz using a square-wave function for V_{AC} . To study the oscillations in the time-domain, we performed a series of time-resolved PL measurements using an avalanche photodiode (APD).⁴⁷ The general measurement procedures are as follows: first, we choose a mechanical resonance, indicated by line broadening in time-integrated PL (here, we also chose a trion emission line); then, a monochromator is used to spectrally filter the emission in adjacent spectral windows and the photons are detected by an APD using the time correlated single-photon counting electronics triggered by the function generator (see the [supplementary material](#) for details). Finally, we collect all the data (three-dimensional matrix of wavelength-time-photon count) and plot the color-coded time-resolved (phase-locked) QD emission shift.

The result for a driving frequency of 19.75 MHz is shown in [Fig. 4\(a\)](#). The maximum resonant frequency that we observed was around 61.5 MHz, see [Fig. 4\(b\)](#). We note that in this experiment, the rate at which the emission energy shifts exceeds values of $50 \mu\text{eV/ns}$. Taking into account the fact that the typical lifetime of the excitonic transitions in the state-of-the-art GaAs QDs is of the order of 250 ps and the corresponding natural linewidth is $2.3 \mu\text{eV}$, this means that the strain modulation produces energy shifts of the order of 5 times the natural linewidth during the lifetime of the exciton. As strain also changes the excitonic fine-structure splitting,^{48,49} this speed may be already sufficient to observe nontrivial phenomena, such as Landau-Zener transitions.^{50,51} Another application scenario is to use mechanical oscillations to control the state of a single spin confined in a QD via g-tensor modulation techniques at constant magnetic fields.⁵² In fact, it has been recently found out that the g-tensor of holes confined in QDs reacts sensitively to strain.^{27,53} Compared to electric-field based g-tensor modulation, a strain-field g-tensor modulation may be beneficial because of reduced hole dephasing produced by charge noise.⁵⁴

In conclusion, we have investigated here the possibility of using micromachined piezoelectric actuators to tune the frequency of

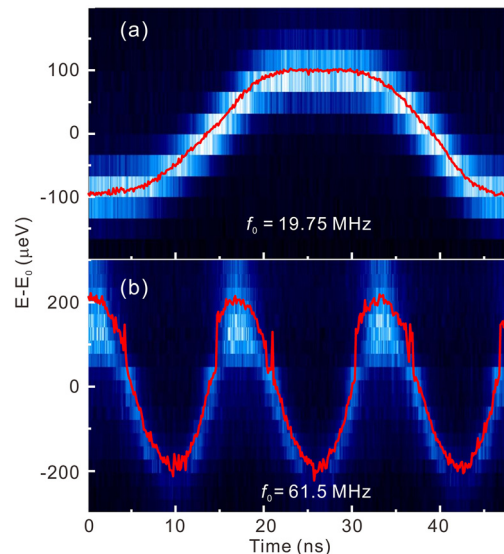


FIG. 4. Time-resolved PL evolution of the exciton emission of a GaAs QD driven with a square wave with resonance frequency f_0 at (a) 19.75 MHz and (b) 61.5 MHz with a driving voltage of $V_0 = 1.9$ V and a DC voltage of $V_{DC} = 0$. The red solid lines are the peak position extracted from Lorentz fits of the PL emission at a fixed time.

oscillations in micromechanical resonators consisting of semiconductor nanomembranes with embedded QDs. For a proof-of-principle, we have used simple nanomembrane beam-oscillators directly bonded onto the actuator, which we use to both drive vibrations and control their resonant frequency. If required, tuning ranges substantially higher than those reported here are in principle possible, provided that the fabrication and stability of the mechanical resonances are improved. To this end, we envision having (i) the mechanical resonator suspended on a well-defined rigid frame bonded to the PMN-PT actuator and/or (ii) the oscillations driven via a more localized mechanical excitation method such as radiation pressure or surface acoustic waves. This approach would open up the possibility to tune the resonant frequency of state-of-the-art optomechanical resonators, such as those based on silicon-nitride.⁵⁵ Due to the possibility of operating the actuators in vacuum and at low temperature, the approach is more flexible than the cantilever-bending method and may be a useful alternative to on-chip electrostatic actuation for fine-control of the resonance frequency of advanced optomechanical resonators operated in the quantum regime.

See the [supplementary material](#) for the multilayer structures used in this work, an additional plot of the relation between resonant frequency f_0 and emission energy of a trion from one In(Ga)As QD in another nanomembrane, the schematic experimental setup for time-resolved measurements, and frequency scans of the PL emission from QDs located in nominally identical membranes.

This work was supported by the FWF (P 29603), the Linz Institute of Technology (LIT), the LIT Secure and Correct Systems Lab funded by the state of Upper Austria, the EU project HANAS (No. 601126210), AWS Austria Wirtschaftsservice (PRIZE Programme, Grant No. P1308457), the European Research council (ERC) under the European Union's Horizon 2020 Research and Innovation Programme (SPQRel, Grant Agreement No. 679183), and the German Excellence Initiative via the Cluster of Excellence Nanosystems Initiative Munich (NIM). X. Yuan acknowledges support of the China Scholarship Council (CSC, No. 201306090010). Y. Huo thanks support of NSFC (No. 11774326) and STCSM (Nos. 17ZR1443900 and 17PJ1409900). J.M.-S. acknowledges support through the Clarín Programme from the Government of the Principality of Asturias and a Marie Curie-COFUND European grant (No. PA-18-ACB17-29). The authors thank M. Reindl and D. Huber for help with the processing and optical characterization and A. Halilovic, A. Schwarz, S. Bräuer, U. Kainz, and E. Vorhauer for the technical support.

REFERENCES

- ¹J. Chan *et al.*, *Nature* **478**, 89 (2011).
- ²R. Riedinger *et al.*, *Nature* **556**, 473 (2018).
- ³I. Wilson-Rae, P. Zoller, and A. Imamoglu, *Phys. Rev. Lett.* **92**, 075507 (2004).
- ⁴P. Treutlein, C. Genes, K. Hammerer, M. Poggio, and P. Rabl, *Cavity Optomech* (Springer, Berlin/Heidelberg, 2014), pp. 327–351.
- ⁵E. R. Macquarrie *et al.*, *Phys. Rev. Lett.* **111**, 227602 (2013).
- ⁶R. Ruskov, K. Schwab, and A. N. Korotkov, *Phys. Rev. B* **71**, 235407 (2005).
- ⁷S. A. McGee *et al.*, *Phys. Rev. A* **87**, 053818 (2013).
- ⁸N. Vostrosablin, A. A. Rakhubovsky, and R. Filip, *Phys. Rev. A* **94**, 063801 (2016).
- ⁹M. Zhang *et al.*, *Appl. Phys. Lett.* **105**, 051904 (2014).
- ¹⁰G. O. Luiz *et al.*, *Opt. Express* **25**, 31347 (2017).
- ¹¹G. Heinrich *et al.*, *Phys. Rev. Lett.* **107**, 043603 (2011).
- ¹²M. Zalalutdinov *et al.*, *Appl. Phys. Lett.* **83**, 3281 (2003).
- ¹³M. Zhang *et al.*, *Phys. Rev. Lett.* **109**, 233906 (2012).
- ¹⁴W. M. Zhang *et al.*, *Sensors* **15**, 26478 (2015).
- ¹⁵M. A. A. Hafiz, L. Kosuru, and M. I. Younis, *Nat. Commun.* **7**, 11137 (2016).
- ¹⁶G. S. Wiederhecker *et al.*, *Opt. Express* **19**, 2782 (2011).
- ¹⁷R. Perahia *et al.*, *Appl. Phys. Lett.* **97**, 191112 (2010).
- ¹⁸M. Winger *et al.*, *Opt. Express* **19**, 24905 (2011).
- ¹⁹L. Midolo, A. Schliesser, and A. Fiore, *Nat. Nanotechnol.* **13**, 11 (2018).
- ²⁰Q. P. Unterreithmeier, E. M. Weig, and J. P. Kotthaus, *Nature* **458**, 1001 (2009).
- ²¹H. Pfeifer *et al.*, *Opt. Express* **24**, 11407 (2016).
- ²²J. Rieger *et al.*, *Appl. Phys. Lett.* **101**, 103110 (2012).
- ²³S. C. Masmanidis *et al.*, *Science* **317**, 780 (2007).
- ²⁴X. Yuan *et al.*, *Nat. Commun.* **9**, 3058 (2018).
- ²⁵K. C. Balram *et al.*, *Nat. Photonics* **10**, 346 (2016).
- ²⁶J. Yeo *et al.*, *Nat. Nanotechnol.* **9**, 106 (2014).
- ²⁷S. G. Carter *et al.*, *Phys. Rev. Lett.* **121**, 246801 (2018).
- ²⁸M. Montinaro *et al.*, *Nano Lett.* **14**, 4454 (2014).
- ²⁹F. J. R. Schülein *et al.*, *Nat. Nanotechnol.* **10**, 512 (2015).
- ³⁰M. Metcalfe *et al.*, *Phys. Rev. Lett.* **105**, 037401 (2010).
- ³¹J. R. Gell *et al.*, *Appl. Phys. Lett.* **93**, 081115 (2008).
- ³²G. Piredda *et al.*, *Appl. Phys. A* **125**, 201 (2019).
- ³³C. Heyn *et al.*, *Appl. Phys. Lett.* **94**, 183113 (2009).
- ³⁴Y. H. Huo, A. Rastelli, and O. G. Schmidt, *Appl. Phys. Lett.* **102**, 152105 (2013).
- ³⁵D. Ziss *et al.*, *J. Appl. Phys.* **121**, 135303 (2017).
- ³⁶R. Trotta *et al.*, *Nat. Commun.* **7**, 10375 (2016).
- ³⁷J. Martín-Sánchez *et al.*, *Adv. Opt. Mater.* **4**, 682 (2016).
- ³⁸M. Weiß and H. J. Krenner, *J. Phys. D* **51**, 373001 (2018).
- ³⁹E. D. S. Nysten *et al.*, *J. Phys. D* **50**, 43LT01 (2017).
- ⁴⁰M. Weiß *et al.*, *Phys. Rev. Appl.* **9**, 014004 (2018).
- ⁴¹F. R. Braakman *et al.*, *Appl. Phys. Lett.* **105**, 173111 (2014).
- ⁴²S. S. Verbridge *et al.*, *Nano Lett.* **7**, 1728 (2007).
- ⁴³S. S. Verbridge *et al.*, *J. Appl. Phys.* **99**, 124304 (2006).
- ⁴⁴Q. P. Unterreithmeier, T. Faust, and J. P. Kotthaus, *Phys. Rev. Lett.* **105**, 027205 (2010).
- ⁴⁵M. Bückle *et al.*, *Appl. Phys. Lett.* **113**, 201903 (2018).
- ⁴⁶J. M. L. Miller *et al.*, *Appl. Phys. Rev.* **5**, 041307 (2018).
- ⁴⁷M. Weiß *et al.*, *Appl. Phys. Lett.* **109**, 033105 (2016).
- ⁴⁸M. Gong *et al.*, *Phys. Rev. Lett.* **106**, 227401 (2011).
- ⁴⁹R. Trotta *et al.*, *Phys. Rev. Lett.* **109**, 147401 (2012).
- ⁵⁰R. Blattmann *et al.*, *Phys. Rev. A* **89**, 012327 (2014).
- ⁵¹R. K. Malla and M. E. Raikh, *Phys. Rev. B* **97**, 035428 (2018).
- ⁵²Y. Kato *et al.*, *Science* **299**, 1201 (2003).
- ⁵³H. M. G. A. Tholen *et al.*, *Phys. Rev. B* **94**, 245301 (2016).
- ⁵⁴J. Houel *et al.*, *Phys. Rev. Lett.* **112**, 107401 (2014).
- ⁵⁵K. Y. Fong *et al.*, *Appl. Phys. Lett.* **97**, 073112 (2010).